Static quark potential in three flavor QCD

Claude Bernard
Department of Physics, Washington University, St. Louis, Missouri 63130

Tom Burch, Kostas Orginos, and Doug Toussaint
Department of Physics, University of Arizona, Tucson, Arizona 85721

Thomas A. DeGrand
Physics Department, University of Colorado, Boulder, Colorado 80309

Carleton DeTar
Physics Department, University of Utah, Salt Lake City, Utah 84112

Steven Gottlieb
Department of Physics, Indiana University, Bloomington, Indiana 47405

Urs M. Heller
CSIT, Florida State University, Tallahassee, Florida 32306-4120

James E. Hetrick
Department of Physics, University of the Pacific, Stockton, California 95211-0197

Bob Sugar
Department of Physics, University of California, Santa Barbara, California 93106
(Received 25 February 2000; published 7 July 2000)

We study the effects of dynamical quarks on the static quark potential at distances shorter than those where string breaking is expected. Quenched calculations and calculations with three flavors of dynamical quarks are done on sets of lattices with the lattice spacings matched within about one percent. The effect of the sea quarks on the shape of the potential is clearly visible. We investigate the consequences of these effects in a very crude model, namely solving Schrödinger's equation in the resulting potential.

PACS number(s): 11.15.Ha, 12.38.Gc

I. INTRODUCTION

One of the conceptually simplest things that can be computed in lattice QCD is the potential between a static, infinitely heavy quark and antiquark [1]. This potential is used in phenomenological approaches to hadron physics, and is also commonly used in lattice studies to determine the lattice spacing, or overall energy scale. In this work, we explore the differences between the potential computed in the quenched approximation and in full QCD.

In general, there are two main effects. The more dramatic effect of dynamical quarks is the breaking of the string at large distances caused by shielding of the static sources by dynamical quarks. This string breaking is difficult to see in straightforward potential calculations, although studies using both ''string'' type operators and ''meson-meson'' type operators show the expected behavior [2]. We do not consider it here. The second effect is that at shorter distances the dynamical quarks will change the shape of the potential. Roughly speaking, this happens because the quarks reduce the QCD beta function. This means that as we go to shorter distances, the coupling constant in full QCD will not decrease as quickly as in quenched QCD, so the force between the static sources will be larger in full QCD. This effect is the subject of this paper.

This difference is responsible for a shift of the hyperfine splitting in quarkonia. In potential models, the splitting is proportional to the strong coupling constant and to the square of the wave function at the origin, which is greater in the full theory because the coefficient of the beta function is smaller [3]. The same effect has been discussed as an explanation for differences in heavy-light pseudoscalar decay constants, f_B and f_{B_S}, between full and quenched QCD [4]. The idea is that the deeper full QCD potential at the origin will increase the wave function of the light quark in a potential model, hence increasing the amplitude for it to annihilate with the heavy quark.

When one describes the effects of the number of flavors on some physical quantity, one is making an implicit assumption that some other physical parameter is being held constant as the number of dynamical flavors is varied. We are also interested in a variation of this problem—we would like to use a quantity determined from the heavy quark potential as the parameter which is held constant while other physical parameters are compared. To do this, we have to keep in mind that quenched QCD and full QCD with different numbers of dynamical quark flavors are different theories. The potentials of these theories have different shapes. It is impossible to determine the relative length scales in the different theories by matching the entire potential. Instead,

TABLE I. Simulations used in this paper. The first six columns are the sea quark mass(es), the gauge coupling, the number of simulation time units in the run, the number of configurations for which the potential was calculated, the size of the molecular dynamics time step, and the approximate number of conjugate gradient iterations used in the computation of the fermion force. The remaining columns give r_1, r_0 and σ in units of the lattice spacing, and the lattice spacing in fermi, using $r_1 = 0.36$ fm to set the scale. The quenched runs were done with a combination of overrelaxation and heat bath steps, using ten sweeps between samples, with each sweep consisting of four overrelaxation steps and one heatbath step.

$am_l(/m_h)$	$10/g^2$	traj.	N_{conf}	ϵ	CG	r_1/a	r_0/a	σa^2	a(fm)
∞	8.40	na	38	na	na	3.739(19)	5.149(32)	0.0519(8)	0.0969(5)
∞	8.00	na	408	na	na	2.664(6)	3.663(13)	0.1028(10)	0.1360(3)
0.40	7.35	2004	330	0.03	29	2.661(7)	3.672(15)	0.1016(11)	0.1362(4)
0.20	7.15	2070	341	0.03	46	2.703(7)	3.746(14)	0.0966(10)	0.1341(3)
0.10	6.96	2064	339	0.03	81	2.687(10)	3.776(19)	0.0924(12)	0.1349(5)
0.05	6.85	2500	416	0.02	127	2.679(11)	3.808(22)	0.0888(14)	0.1353(5)
0.03/0.05	6.81	1346	224	0.02	214/143	2.651(14)	3.766(29)	0.0909(19)	0.1367(7)
0.02/0.05	6.79	1234	200	0.013	255/127	2.667(13)	3.825(28)	0.0865(17)	0.1359(6)

one must make a choice—for example, determining the lattice spacing from the string tension σ or from Sommer's parameter r_0 [5]. If the couplings of full and quenched simulations are tuned by matching one such parameter, they will differ in the other parameters.

In order to isolate the effects of dynamical quarks, we have done a series of simulations of quenched QCD and three-flavor QCD with a range of quark masses, with the gauge couplings tuned to match the lattice spacing, using one of the possible choices of definitions of the length scale. We used a Symanzik improved gauge action and, in the full QCD runs, an improved Kogut-Susskind quark action that greatly improves the scaling of physical quantities [6–13]. The full QCD simulations were done with an optimized version of the updating algorithm for general quark actions described in Ref. [9]. Most of the results presented here come from a series of runs with three degenerate quarks with masses ranging from approximately the strange quark mass to eight times this mass. We also include some results from shorter runs with two lighter flavors and one quark mass fixed at the strange quark mass. The lattice size was $20^3 \times 64$, or a physical spatial volume of $(2.7\ \text{fm})^3$, with the exception of a finer lattice quenched run which was done on a $28^3 \times 96$ lattice. Some of the parameters of these simulations are tabulated in Table I. Lattice spacings are determined with fractional errors ranging from 0.2 percent for the quenched run to 0.6 percent, and the lattice spacings are matched with a fractional RMS spread of 0.6 percent.

The static quark potential including effects of sea quarks has been calculated by the SESAM/TχL [14], SCRI [15], UKQCD [16] and CPPACS [17] collaborations and by Tamhankar and Gottlieb [18]. The SESAM calculation used the plaquette gauge action and two flavors of Wilson quarks, with a fixed gauge coupling $(6/g^2 = 5.6)$ for the dynamical runs. The SCRI group used two flavors, with both Wilson and Kogut-Susskind quarks, at fixed gauge couplings. The UKQCD calculation used the plaquette gauge action and two flavors of quarks with the Wilson-clover action and the gauge coupling was tuned to match the lattice spacings. The CPPACS calculation used an improved gauge action with two flavors of Wilson-clover quarks, varying the sea quark mass at fixed gauge coupling. Both the UKQCD and CPPACS groups observed an increase in the coefficient of the Coulomb term due to the dynamical quarks. Because we are using three flavors of sea quarks, our results cannot be quantitatively compared with these two flavor results.

II. THE SIMULATIONS

As mentioned above, a choice must be made when deciding how to tune the lattice spacing. The most common choice in recent work is to use the parameter r_0 defined by $r_0^2 F(r_0) = 1.65$, with $r_0 \approx 0.50$ fm. This choice was motivated by the observation that phenomenological studies of the potentials give consistent results for the force at this distance [5]. However, as noted in the original work [5], in principle $r^2 F(r)$ can be set to any number. In these simulations, we are faced with the challenge of tuning the coupling with minimal effort, so it is important that the length scale we choose be accurately measurable in a small simulation. This motivates us to choose a variant which we unimaginatively call r_1, defined by $r_1^2 F(r_1) = 1$. Figure 1 shows the fractional accuracy with which the lattice spacing could be determined in a short simulation for different choices of the constant in $r^2 F(r) = C$. These are plotted as a function of the distance at which the condition is satisfied. The square in this plot indicates the conventional choice $C = 1.65$, and the octagon shows our choice $C = 1.0$. The arrow on the right side shows the accuracy obtained from the string tension. The reason for the improvement in accuracy is that the potential is more accurately determined at shorter distances. However, at very short distances the potential is dominated by the $-\alpha(r)/r$ part, and in this regime a length scale could only be determined by the small dependence of $\alpha(r)$ on r. Thus, the optimal choice for C satisfies $r^2 F(r) = C$ at roughly the distance where the force turns over from Coulomb-like to σr.

We computed the static potential by gauge fixing the lat-

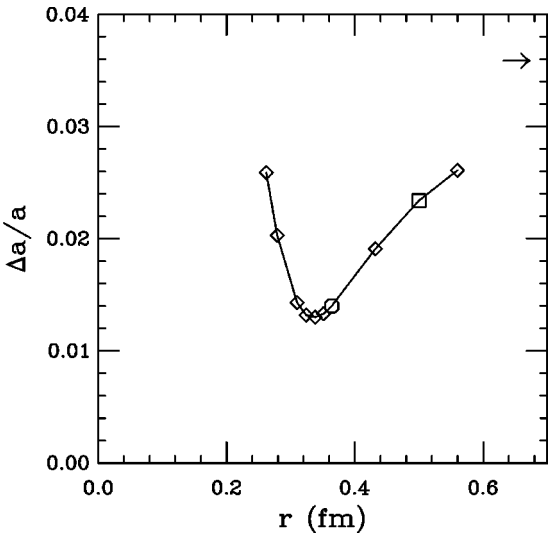

FIG. 1. Accuracy of a lattice spacing determination from the static potential as a function of the distance at which the force is determined. The square is the point where $r^2F(r)=1.65$ and the octagon the point where $r^2F(r)=1$. The arrow is the accuracy of a string tension determination.

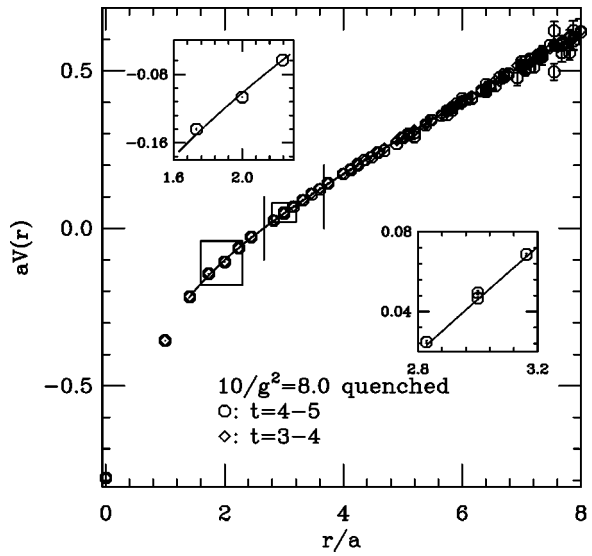

FIG. 2. The static quark potential in quenched QCD, with $10/g^2_{imp}=8.0$. Octagons are from time separation four to five, and diamonds from time separation three to four. The solid line is the Coulomb plus linear fit to the potential. Insets show the remaining lattice artifacts, as explained in the text. A constant has been subtracted from the potential to set $V(r_1)=0$. The vertical lines are at r_1 and r_0.

tices to the Coulomb gauge and then just computing products of the temporal links. This is effectively a smeared spatial string operator, smeared over the distance scale at which the QCD dynamics correlates the links, but we have made no further attempt to optimize our static pair creation operator. The potential was determined from the ratios of ''loops'' at time separations four and five (five and six for the $a\approx 0.10$ quenched run). Ratios of distances three and four gave results which in some cases differed from the ratios at times 4-5 by more than the statistical error, while inclusion of larger distances in a fit did not appreciably improve the statistical errors. After the potential was computed at all spatial separations, separations related by lattice symmetries were combined. Then the potential was fit to the form $V(r)=C-\alpha/r+\sigma r$. This form gave good results for separations from (1,1,0) to the largest values for which we could compute the potential. Our quoted results are obtained to fits from all points at spatial distances from $\sqrt{2}a$ to $6a$, with the exception of the $a\approx 0.10$ fm run, where distances up to $7a$ were used. r_0 and r_1 were derived from α and σ. Such a simple approach to fitting the potential is only possible because the improved action suppresses most of the lattice artifacts. Figure 2 shows the potential for the quenched run, where our statistics are largest, together with the fit that was found. A remaining lattice artifact is visible at distance two [separation (2,0,0)], where the potential is visibly below the smooth curve. An elegant test for lattice artifacts is to compare the two points at distance three, at separations (3,0,0) and (2,2,1), which are shown in an inset in Fig. 2. For the quenched potential there is a small discrepancy here, with the ''on-axis'' point lower. For most of our full QCD runs this discrepancy is smaller than the statistical errors. For the quenched case we have done a shorter simulation at a smaller lattice spacing, $a\approx 0.10$ fm, to check for dependence on the lattice spacing. This run was done on $28^3\times 96$ lattices at $10/g^2=8.4$. Figure 3 shows the short distance part of the potential for the quenched theory at the two lattice spacings, showing excellent agreement. Since the main point of this work is to isolate the effects of dynamical quarks, we have not included a systematic error from the remaining lattice

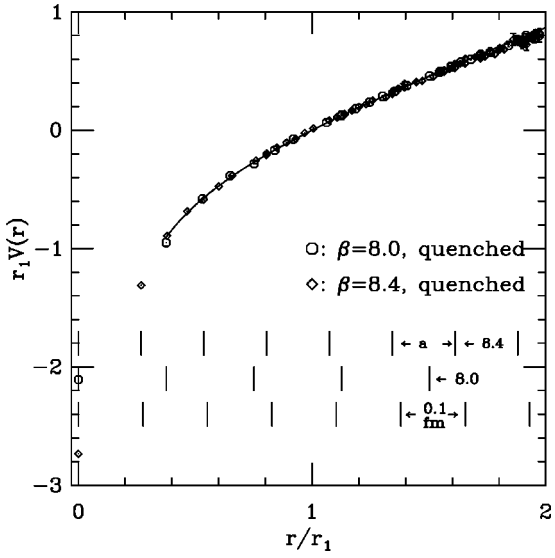

FIG. 3. The short distance part of the static quark potential in quenched QCD for two different lattice spacings. Octagons are from the $10/g^2=8.0$ run, and diamonds from the $10/g^2=8.4$ run. The solid lines are the Coulomb plus linear fit to the potentials, plotted in units of r_1. The upper two sets of vertical lines show the lattice spacings—a, $2a$ ... —for the two runs, and the lower set is at spacings of 0.1 fm, where the overall length scale was set by $r_0=0.50$ fm.

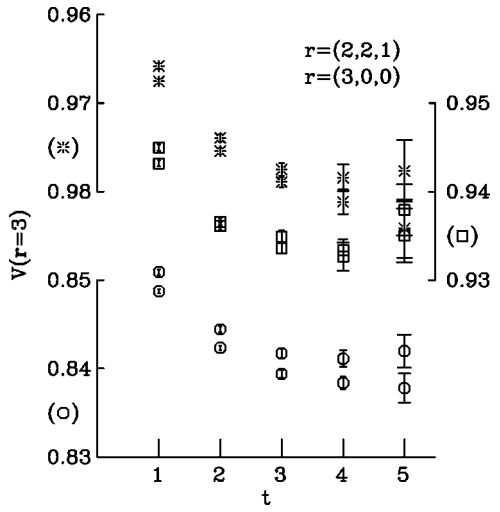

FIG. 4. The ''potential'' $(-\log[W(r,t+1)/W(r,t)])$ as a function of time separation. Here the spatial distance is three, and we show results from separation vectors (2,2,1) and (3,0,0). The octagons are the quenched potential, the squares the potential at $am_q=0.1$, and the bursts the potential at $am_q=0.05$.

artifacts in our quoted error estimates. First, we think that this error is small. But more importantly, we are comparing quenched and full QCD lattices at matched lattice spacings, and these systematic errors will largely cancel in the differences of the two. (All of our runs show essentially the same discrepancy at distance two, for example.) In Figs. 4 and 5 we show in more detail the effects of the choice of time interval for determining the potential, and the remaining breaking of rotational symmetry. Figure 4 shows $V_{eff}(r,t) = -\log[W(r,t+1)/W(r,t)]$ at spatial distance three as a function of time for the quenched run and two of the three-flavor runs. Values for the different quark masses were shifted vertically to aid comparison. The vertical scales are labeled with parenthesized symbols for the corresponding quark mass. As discussed above, at this distance we have two separation vectors, (2,2,1) (upper point in each pair) and (3,0,0) (lower points). It can be seen that the breaking of rotational invari-

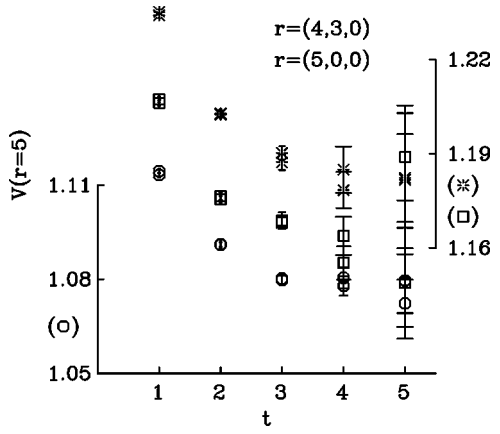

FIG. 5. The same as Fig. 4, but at a spatial distance of five. We show results from separation vectors (4,3,0) and (5,0,0). Symbols are the same as in Fig. 4.

TABLE II. Accuracy and consistency of the lattice spacing determination from fitting all points and from the method of Ref. [5] applied along three different axes. For the method of Ref. [5] the second column shows the direction along which interpolation was done.

Quantity	Method	Value	Fractional error
r_0/a	FIT	3.663(13)	0.0034
r_0/a	(1,0,0)	3.666(21)	0.0057
r_0/a	(1,1,0)	3.691(27)	0.0074
r_0/a	(1,1,1)	3.876(93)	0.0240
r_1/a	FIT	2.664(6)	0.0023
r_1/a	(1,0,0)	2.650(9)	0.0033
r_1/a	(1,1,0)	2.661(14)	0.0051
r_1/a	(1,1,1)	2.692(19)	0.0069

ance and the remaining systematic error from excited states are approximately the same for the quenched and three-flavor runs. Figure 5 shows the same thing at a spatial distance of five, in the upper part of the range we used for fitting. Again, we have two separation vectors, (4,3,0) and (5,0,0), but at this distance there are no significant differences between the potentials at these two vectors. We have done some fits to these plots including an excited state, and find results consistent with our choice of using $t=4$ to 5. However, this fitting procedure did not produce any significant decrease in the errors for the potential.

As detailed in Table I, we were able to choose values of the gauge coupling to match r_1 in the different runs with a fractional RMS spread of 0.6 percent, with the final lattice spacings known with accuracies ranging from 0.2 percent for the quenched run to 0.6 percent for the lowest mass run.

Our procedure for determining the lattice spacing differs from that used in Ref. [5] (see also [19]), where an interpolation is done using values of the potential along one axis, using a tree level calculation of the potential to correct for lattice artifacts. We have compared the results of the different methods using our large $10/g^2=8.0$ quenched sample. In Table II we tabulate r_0/a and r_1/a calculated using our fitting procedure and by the procedure of Ref. [5] applied along the lattice directions (1,0,0), (1,1,0) and (1,1,1). The results are consistent, with r_1/a better determined than r_0/a for both methods. The fitting method produces smaller statistical errors simply because it makes use of the potential at all possible separations.

All of the errors quoted in this paper are statistical errors obtained with the jackknife method.

III. EFFECTS OF SEA QUARKS

In Fig. 6, we plot the quenched potential and the potential with three degenerate flavors of quarks at $am_q=0.05$. This is approximately the mass of the strange quark. Both the distance scale and the potential are plotted in units of r_1, and a constant has been subtracted from the potential so that it is zero at r_1. Since r_1 was determined from this potential, this results in matching the slope of the potentials at $r=r_1$, so the

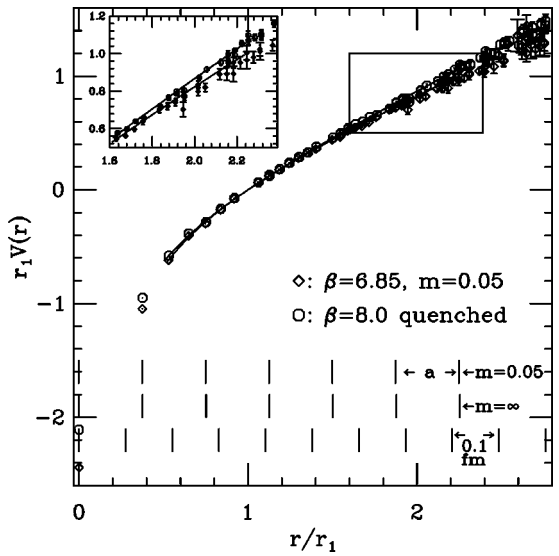

FIG. 6. The static quark potential for quenched (octagons) and three flavor (diamonds) QCD, in units of r_1. The solid lines are fits to the Coulomb plus constant plus linear form. The lattice spacing was matched using r_1 as described in the text. As in Fig. 3, the upper two rulers show the lattice spacing in the two runs, and the lower one shows units of 0.1 fm.

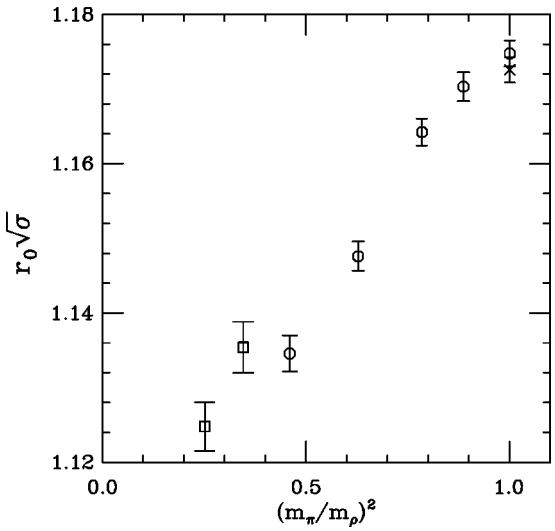

FIG. 7. Effects of dynamical quarks on the shape of the potential. Here we plot $r_0\sqrt{\sigma}$ as a function of the quark mass. The quenched points are at the right, with the octagon coming from the $10/g^2=8.0$ run and the cross from the $10/g^2=8.4$ run. The remaining octagons are full QCD runs with three degenerate flavors, and the squares are full QCD runs with two light flavors and one heavy.

fits are tangent at this point. Away from the point where the force is matched, the potentials have different slopes, as expected. In particular, at shorter distances the force is larger in full QCD, as expected since the coupling ''runs'' more slowly. This graph contains three ''rulers.'' The upper sets of vertical lines show the lattice spacings for the dynamical and quenched runs, and the lower set is at spacings of 0.1 fm, where the overall length scale was set by $r_0=0.50$ fm in the quenched run.

As a quantitative measure of the change in the shape of the potential due to the dynamical quarks, we may plot dimensionless quantities such as $r_0\sqrt{\sigma}$ or $r_1\sqrt{\sigma}$. Figures 7 and 8 show these two quantities as a function of quark mass, where $(m_\pi/m_\rho)^2$ is used as an indicator of the quark mass. The effect of the sea quarks is clear, and it should be noted that the effect is appreciable even for fairly heavy sea quarks. (The dependence of these quantities on the sea quark mass emphasizes that only one dimensionful quantity can be matched in tuning full and quenched simulations to match the lattice spacing.) Figure 7 can be compared with Fig. 1 of Ref. [14], which plots the same quantity with two flavors of Wilson quarks. We note in passing that an extrapolation of Fig. 7 to light quark mass is consistent with commonly used values for r_0 and $\sqrt{\sigma}$: 0.50 fm$\times$440 MeV$=1.12$.

IV. PHENOMENOLOGICAL CONSEQUENCES

The larger quark-antiquark force at small distances in full QCD has been suggested as a qualitative explanation for some of the differences between quenched and full QCD that have been found in simulations. For example, there is some indication that dynamical quarks increase the value of f_B and f_{B_S} [20–23], which can be understood as a larger wave function at the origin due to the deeper short distance potential well in full QCD [4]. Also, dynamical quarks are expected to increase the spin splittings in heavy quarkonia [3,24,25], which can again be considered to result from a smaller wave function.

To make a crude estimate of these effects, we have solved the nonrelativistic Schrödinger equation for the ground state in the static potentials. Of course, we do not advocate this as a replacement for a real solution to QCD, but in the spirit of trying to understand the differences between quenched and full QCD, it is a worthwhile exercise. Specifically, we used

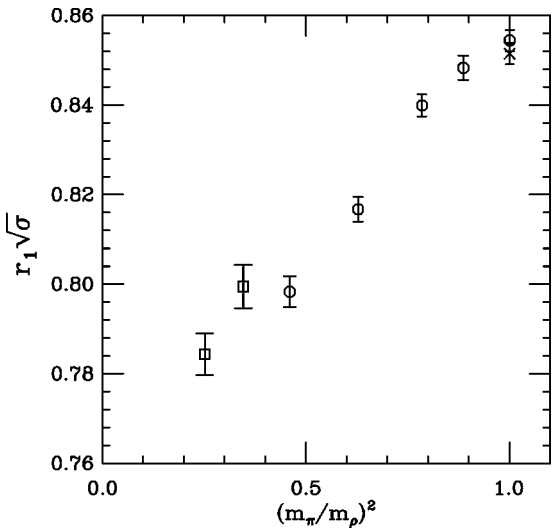

FIG. 8. The same as Fig. 7, except we plot $r_1\sqrt{\sigma}$. Physically, the difference is that this is sensitive to shorter distances than the previous plot.

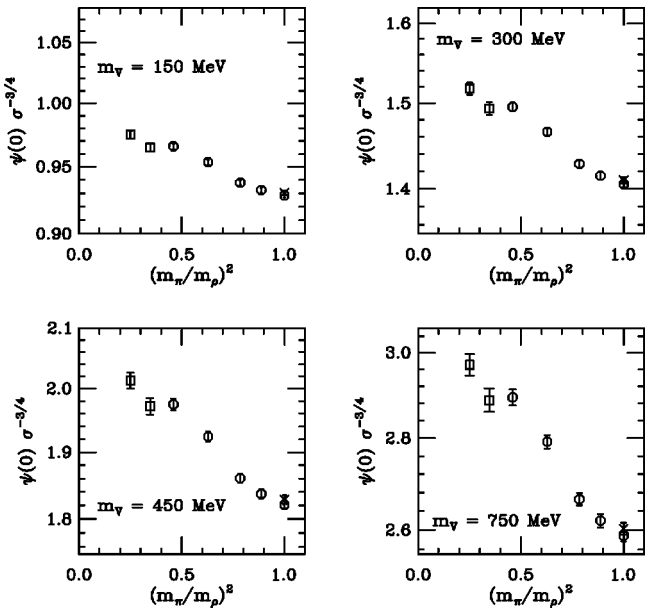

FIG. 9. Wave function at the origin in units of the string tension for valence quark masses of 150, 300, 450 and 750 MeV. The horizontal scale is the sea quark mass, parametrized by $(m_\pi/m_\rho)^2$, placing the quenched calculation at the right side. For the two smallest sea quark masses (squares), there are two light flavors of sea quark and one heavier flavor at about the strange quark mass. The cross indicates the result for the quenched sample with $a \approx 0.10$ fm. The vertical scale for each graph covers a range of twenty percent.

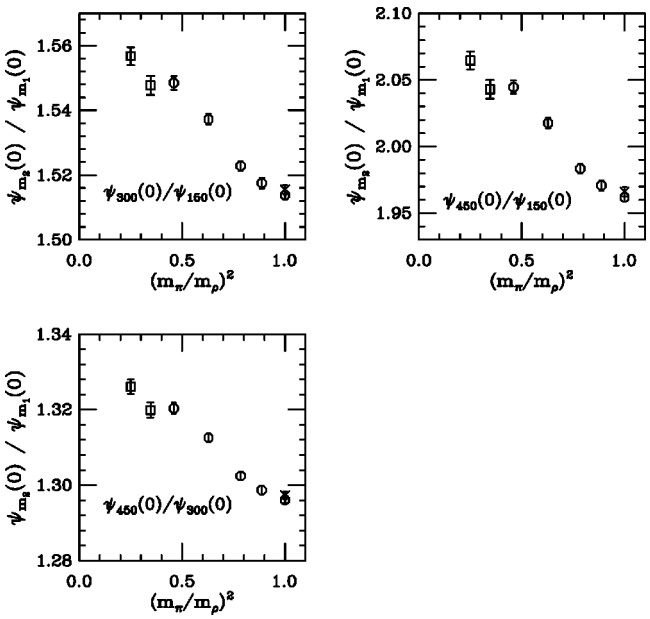

FIG. 10. Ratios of wave function at the origin for different valence quark masses. The horizontal axis and symbols are the same as in Fig. 9. The three panels show $\Psi_{300}(0)/\Psi_{150}(0)$, $\Psi_{450}(0)/\Psi_{150}(0)$ and $\Psi_{450}(0)/\Psi_{300}(0)$, respectively. These can be *very* loosely interpreted as f_B/f_π, f_{B_S}/f_π and f_{B_S}/f_B. Note that in this figure the three panels cover different fractional ranges.

the fitted Coulomb plus linear plus constant form for the potential. Alternative approaches, where we connected the points in the potential by straight lines or solved a discrete lattice version of the Schrödinger equation, gave similar results. We show the ''Coulomb plus linear'' results because we expect that this is closer to continuum physics than the discrete lattice potential, which is finite even at $r=0$. However, it must be remembered that this $1/r$ term is phenomenological, not fundamental. (We are working at distances too large to identify it with a perturbative potential, and too short to identify it with a universal correction to the linear potential.) For light valence quark masses the wave function extends beyond the region where we have fit the potential and into the region where we would expect string breaking to show up. By using the fitted form of the potential, we are ignoring this effect. Conversely, for heavy valence quark masses the wave function is small, and sensitive to the treatment of the short distance potential. However, with our matched quenched and full QCD lattices, we expect this effect to be the same for the quenched and full potentials. Note that we can use our small sample of quenched lattices with $a \approx 0.1$ fm to test the sensitivity to the lattice artifacts.

To repeat, a comparison of a dimensionful quantity between quenched and full QCD can only be made subject to a choice of the quantity used to determine the length scale in the quenched theory. For example, if we choose the string tension, then we might compare the wave functions at the origin in units of the string tension, or $\Psi(0)\sigma^{-3/4}$.

We solved Schrödinger's equation for valence quark masses of 150, 300, 450 and 750 MeV. These can be regarded as constituent quark masses for, respectively, a light-light meson reduced mass (this is a stretch), a heavy-light meson, a heavy-strange meson, and charmonium reduced mass. Figure 9 shows the ground state wave function at the origin in units of the string tension for these four masses as a function of the sea quark mass, parametrized by $(m_\pi/m_\rho)^2$. As expected, the larger force at short distance results in a larger wave function at the origin in full QCD. This is consistent with indications that the inclusion of dynamical quarks increases decay constants (f_B and f_{B_S}) [20–23] and hyperfine splittings in quarkonia [3,24,25]. This figure also shows $\Psi(0)$ from the quenched $a \approx 0.10$ fm run. As expected, the effect of decreasing the lattice spacing is larger for the heavier quark masses. As can be seen from Fig. 7, Fig. 9 would look quite different if we chose r_0 or r_1 to set the scale. For example, at $m_q = 150$ MeV, the wave function in units of r_0 increases by less than one percent as the sea quark mass is lowered to $0.02/a$, while in units of σ it increases by almost five percent.

An alternative approach is to use the wave function for light quarks to set the scale. This is similar to using f_π to fix the lattice spacing, as was done for example in the calculations of f_B in Ref. [21]. Then we plot the ratios of wave functions for different valence quark masses as functions of the sea quark masses in Fig. 10. Again, the dependence on sea quark mass is clearly visible, but the size of the effect is much smaller than when the string tension sets the scale. For example, $\Psi(0)\sigma^{-3/4}$ at $m_V = 300$ MeV increases by 6.3 $\pm 0.5\%$ with three degenerate flavors of sea quark with

$(m_\pi/m_\rho)^2 = 0.46$, or about the strange quark mass. However, the ratio of wave functions $\Psi_{300}(0)/\Psi_{150}(0)$ increases by only $2.2 \pm 0.2\%$.

ACKNOWLEDGMENTS

Computations were done on the Origin 2000 clusters at LANL, on the T3E at NERSC, on the T3E, SP2 and SP3 at SDSC, on the NT cluster and Origin 2000 at NCSA, on the Origin 2000 at BU and on the PC cluster at Indiana University. This work was supported by the U.S. Department of Energy under contracts DOE DE-FG02-91ER-40628, DOE DE-FG03-95ER-40894, DOE DE-FG02-91ER-40661, DOE DE-FG05-96ER-40979 and DOE DE-FG03-95ER-40906 and National Science Foundation grants NSF PHY99-70701 and NSF PHY97-22022.

[1] For a current review, see G. Bali, hep-ph/0001312.
[2] A recent summary may be found in K. Schilling, in *Lattice '99*, Proceedings of the 17th International Symposium, Pisa, Italy, 1999 [Nucl. Phys. B (Proc. Suppl.) **83-84**, 140 (2000); also see F. Knechtli, *ibid.* p. 673; C.E. DeTar, U.M. Heller, and P. Lacock, *ibid.* p. 310; F.D.R. Bonnet, D.B. Leinweber, A.G. Williams, and J.M. Zanotti, hep-lat/9912044; UKQCD Collaboration, P. Pennanen and C. Michael, hep-lat/0001015.
[3] A.X. El-Khadra, G.M. Hockney, A.S. Kronfeld, and P.B. Mackenzie, Phys. Rev. Lett. **69**, 729 (1992); A.X. El-Khadra, in Proceedings of Lattice '92 [Nucl. Phys. B (Proc. Suppl.) **30**, 449 (1993)].
[4] The relation between between the pseudoscalar decay and the wave function at the origin in a quark model goes back to R. Van Royen and V.F. Weisskopf, Nuovo Cimento A **50**, 617 (1967); **51**, 583 (1967). The fact that this would imply a decrease in decay constants due to quenching has been noticed many times. See, for example, F. Butler *et al.*, Nucl. Phys. **B421**, 217 (1994) (for the light-light case), and S. Collins *et al.*, Phys. Rev. D **55**, 1630 (1997) or [21] (for the heavy-light case).
[5] R. Sommer, Nucl. Phys. **B411**, 839 (1994).
[6] C. Bernard *et al.*, Phys. Rev. D **58**, 014503 (1998).
[7] T. Blum *et al.*, Phys. Rev. D **55**, 1133 (1997).
[8] G.P. Lepage, Nucl. Phys. B (Proc. Suppl.) **60A**, 267 (1998).
[9] K. Orginos and D. Toussaint, Phys. Rev. D **59**, 014501 (1999); Nucl. Phys. B (Proc. Suppl.) **73**, 909 (1999).
[10] J.F. Lagäe and D.K. Sinclair, Nucl. Phys. B (Proc. Suppl.) **63**, 892 (1998); Phys. Rev. D **59**, 014511 (1999).
[11] K. Orginos, D. Toussaint, and R.L. Sugar, Phys. Rev. D **60**, 054503 (1999); in *Lattice '99* [2], p. 878.
[12] G.P. Lepage, Phys. Rev. D **59**, 074502 (1999).
[13] MILC Collaboration, C. Bernard *et al.*, Phys. Rev. D **61**, 111502 (2000).
[14] SESAM and TχL Collaborations, G.S. Bali *et al.*, Nucl. Phys. B (Proc. Suppl.) **63**, 209 (1998).
[15] U.M. Heller, K.M. Bitar, R.G. Edwards, and A.D. Kennedy, Phys. Lett. B **335**, 71 (1994).
[16] UKQCD Collaboration, C.R. Allton *et al.*, Phys. Rev. D **60**, 034507 (1999); UKQCD Collaboration, J. Garden, in *Lattice '99* [2], p. 165.
[17] S. Aoki *et al.*, Nucl. Phys. B (Proc. Suppl.) **63**, 221 (1998).
[18] S. Tamhankar and S. Gottlieb, in *Lattice '99* [2], p. 212.
[19] M. Guagnelli, R. Sommer, and H. Wittig, Nucl. Phys. **B535**, 389 (1998).
[20] MILC Collaboration, C. Bernard *et al.*, Nucl. Phys. B (Proc. Suppl.) **47**, 459 (1996).
[21] MILC Collaboration, C. Bernard *et al.*, Phys. Rev. Lett. **81**, 4812 (1998).
[22] S. Collins *et al.*, Phys. Rev. D **60**, 074504 (1999).
[23] CP-PACS Collaboration, A. Ali Khan *et al.*, in *Lattice '99* [2], p. 331; CP-PACS Collaboration, A. Ali Khan *et al.*, *ibid.* p. 265.
[24] T. Onogi *et al.*, Nucl. Phys. B (Proc. Suppl.) **34**, 492 (1994).
[25] CP-PACS Collaboration, A. Ali Khan *et al.*, in *Lattice '99* [2], p. 319.